1992-5-2

CONTROLLING WELD PENETRATION IN GTAW USING VISION SENSING AND ADAPTIVE CONTROL TECHNIQUE

Yuming Zhang
Harbin Institute of Technology
P.O.Box 620
Harbin 150006
China

R. Kovacevic
Center for Robotics and
Manufacturing Systems
University of Kentucky
Lexington, KY40506

L. Wu and *D. H. Chen*
Harbin Institute of Technology
P.O. Box 620
Harbin 150006
China

Abstract

It is found that the back-side weld width in GTAW can be sufficiently represented by the top-side average depression depth. Thus, it is feasible to control the full penetration state (the back-side weld width) based on the measurement and control of the top-side parameters. In order to measure the top-side weld geometric parameters on-line, a real-time image processing technique is proposed for the weld-stripe images. An adaptive predictive decoupling controller is developed. Experiments under a variety of variable welding conditions have been conducted to verify the effectiveness of the developed vision-based top-side full penetration control technique.

Introduction

Researchers have conducted studies to find feasible approaches to control the weld penetration for either full penetration or partial penetration instances, utilizing a top-side sensor. Based upon the concept of using weld pool motion for pool geometry sensing [1,2], much research has been performed [3–7]. However, Hardt [5] and Sorensen [4] have shown that it is not practical to detect the pool shape in partial penetration using the concept of pool oscillation through analysis and experiments. Also, it was demonstrated by Tam and Hardt [6] that in the circumstance of full penetration the unique identification of the pool shape is unreliable if no other correlating data is available. The reflection ultrasound method was utilized to measure the size of the stationary weld pool by Hardt and Katz [8]. Similarly, ultrasonic measurements of the weld pool were performed at the Idaho National Engineering Laboratory [9-12]. In a recent report, an effort to discriminate among different geometries of welds was presented [12]. This report indicated a more realistic noncontacting sensor-based system was under investigation. Studies have been conducted in infrared sensing of welds as well [13,14]. Recently, Chen and Chin utilized an infrared sensing technique to measure the welding temperature distribution [14]. Relationships were obtained between the bead width as well as the depth of joint penetration with respect to the characteristics of the temperature profiles. However, while variable currents were used to produce the variation in penetration, all other experimental variables were held constant. As we know, if welding conditions can be precisely controlled, an open-loop control may produce satisfactory weld penetration utilizing experimentally determined parameters. A closed-loop weld penetration control appears to overcome the disturbances encountered in welding conditions. From this standpoint, relationships obtained based on a wider variety of experimental conditions, which emulate the disturbance in practical welding, will be possibly more appropriate.

The authors observed that a skilled human welder can obtain adequate information on the full penetration state by viewing the end region of the weld pool. If the experience of the skilled human welder can be extracted, the information on the full penetration state can probably be obtained utilizing a machine vision approach. Based on this concept, a top-vision control strategy for full penetration is presented for GTAW.

Top-vision Control Principle

The presented top-vision control is principally shown in Fig.1 where the penetration feedback information is measured through a geometric model, an image processing unit and a 3D vision sensor. The 3D sensor acquires the images of the weld, while the image processing unit processes the images to calculate the top-side geometric parameters of the weld. The geometric model describes the relationship between the back-side weld width (which represents the full penetration state) and the top-side geometric parameters of the weld. According to the set point of the full penetration state and the measured full penetration state, the control signal is produced by the controller to adjust the welding parameters.

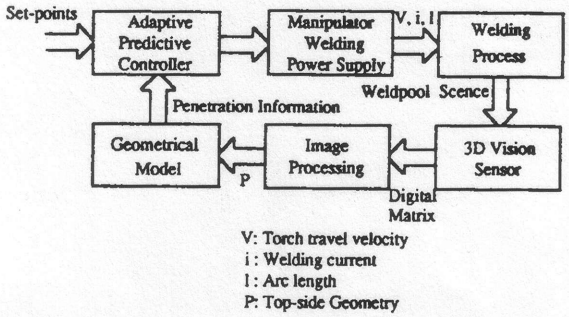

Fig.1 Full-penetration top-side vision-based adaptive control principle

Geometric Description of the Weld Cross Section

A cross section of full penetration weld is shown in Fig.2 where L_1–L_4 are straight lines, and c_1 and c_2 are formed due to the depression. In general, the top-side depression depth H, the top-side weld width b, the back-side depression depth H_b and the back-side weld width b_b are used to describe the cross section geometrically.

Let us introduce a new geometric parameter, called the average depression depth. The top-side average depression depth h is defined as $h=S/b$. The back-side average depression depth h_b can be defined similarly. By h, the back-side weld width can be sufficiently represented in a simple linear model (the detail can be found later in this paper).

In the following section, we turn to the measurements of the top-side geometric parameters.

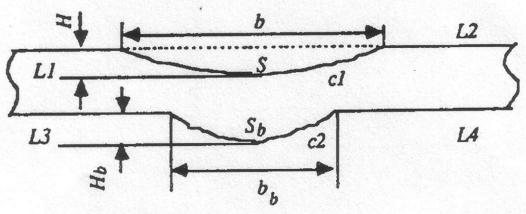

Fig.2 Cross section of a full penetration weld

Yuming Zhang is currently a visiting scholar in the Center for Robotics and Manufacturing Systems at University of Kentucky.

Sensing System

The principle of the 3D vision sensing system is schematically shown by Fig.3. In this sensing system, the structured-light plane is produced and projected onto the weld surface by means of a cylindrical lens. When the light plane is projected onto the weld bead, a laser stripe forms. This laser stripe is calibrated so as to be vertical to the weld bead. It can be seen that the laser stripe is the set of the intersected points of the weld surface and the light plane. Thus, the shape information of the cross section of the weld has been included in this laser-stripe which can be acquired based upon the processing of the weld-stripe image on the *xy* image plane (On this plane, *x-axis* and *y-axis* correspond to the transverse and vertical directions, respectively). The main technical data of the sensing system is listed in Table 1.

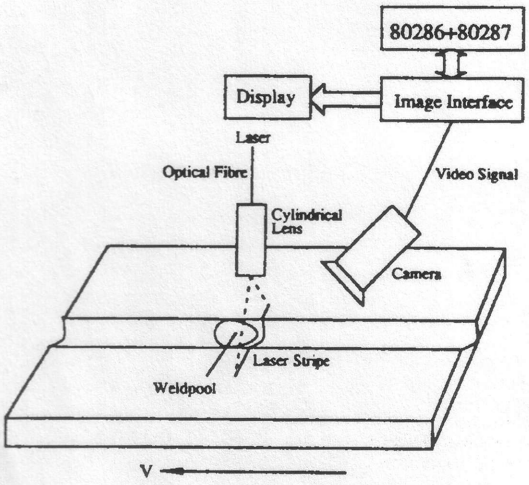

Fig.3 Structured-light 3D vision sensing principle

Table 1 Sensor technical data

Computer	80286+80287
Image Interface	8 bit, 512 X 512, 30 frames per second
Laser source	Nd:YAG, 1.06 μm, 0.1-33w
Optical Filter	wavelength: 10579 $\mathring{A}_o$ half width band: 123 $\mathring{A}$

In order to reject the disturbances due to the arc light and due to the radiation from the hot metal, a narrow band filter is employed. The weld-stripe image is acquired by the camera and then converted into a digital greyscale matrix by means of a real-time image interface.

Although the narrow band optical filter can reject most energy of the arc light and the hot radiation, the disturbances due to the arc light and the hot radiation exist in the image. However, the distance between the end of the weldpool and the laser stripe can not be too large due to the problem of control delay. We selected the distance between the electrode and the laser stripe to be 20mm (about 5mm behind the end of the weldpool).

Real-time Processing of the Weld-stripe Images

Fig.4 shows some typical weld-stripe images where a He-Ne laser is employed for off-line measurements and a Nd:YAG laser for on-line measurements. In general, the following five steps are necessary to acquire the weld geometric parameters from the weld-stripe images: 1) Image filtering or noise suppression; 2) A grey-level into binary image conversion; 3) Medial axis of the laser stripe extraction, i.e., laser stripe thinning; 4) Feature points of the medial axis recognition; 5) Weld geometric parameters computation based on the medial axis and the feature points. The above procedures are time-consuming. Thus, we presented a real-time image processing technique based on our image features, following 1) Adaptive dynamic medial axis extraction; 2) Unbiased feature points recognition; 3) Weld geometric parameters computation. We now first discuss the medial axis extraction.

In order to solve the conflict between the computational speed and the window size, a dynamic thinning procedure (DTP) is proposed based upon the assumption that the laser stripe is continuous. The essence of this procedure is to begin the search for the maximum greyscale point (the set of which along *x-axis* is selected to be the medial axis of the laser stripe) from an initial point which is close to the maximum greyscale point. According to the assumption on the continuity, the vertical coordinate of this initial point can be selected to be the vertical coordinate of the neighboring maximum greyscale point, which is readily available. Thus, if the assumption on the continuity of the laser stripe is true, no more maximum greyscale points are located over a large range except the first one found in each frame image. The computational time will be significantly reduced.

If the continuity assumption is true, the aforementioned DTP will always function properly. However, during actual welding, the continuity of the laser stripe can not be guaranteed. In this case, the DTP will not work properly. In order to overcome the influence of the discontinuity upon the thinning, a modified dynamic thinning algorithm-- the adaptive dynamic thinning algorithm (ADTA)-- is proposed.

The adaptive dynamic thinning algorithm first determines if $(x, y_0^*(x))$ (which is selected by the DTP) is on the laser stripe. If $y_0^*(x)$ is regarded to be on the laser stripe, $(x, y_0^*(x))$ is accepted as a point of the laser stripe, and is denoted by $(x, y_0(x))$. Otherwise, the search for $(x, y_0(x))$ is extended to a large area. Some resulting medial axes can be found in Fig.5.

Experiments reveal the ADTA to be robust to the various disturbances encountered during actual welding. Also, this algorithm can be implemented sufficiently fast so as to be regarded as real-time for our particular control purpose. Examinations show that the computational time is guaranteed to be less than 80 milliseconds on our experimental set-up.

We now discuss how to recognize the feature points based upon the extracted medial axis. The medial axis curve consists of three parts: two straight lines and a curve. The curve corresponds to the weld depression and the two straight lines correspond to the unmolten part of the weld. These three parts are divided by two points, called the feature points of the medial axis. In order to compute the weld geometric parameters accurately, the feature points must be recognized unbiasedly. However, due to the disturbances from the arc light and the radiation of weldpool, it is very difficult to obtain an ideal medial axis of the laser stripe. Furthermore, in many cases, the feature points may not be apparent since the degree of the weld depression is small. As a result, an unbiased recognition algorithm is developed.

Assume a medial axis as shown in Fig.6. Our intention is to determine the horizontal coordinates of the feature points $(a, y_0(a))$ and $(b, y_0(b))$, (i.e., a and b). In the following discussion, only a is considered since b can be recognized in the same manner.

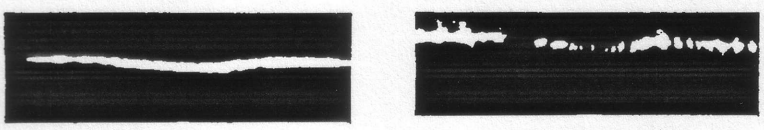

(a) He-Ne laser stripe (b) YAG:Nd laser stripe

Fig.4 Typical weld-stripe images

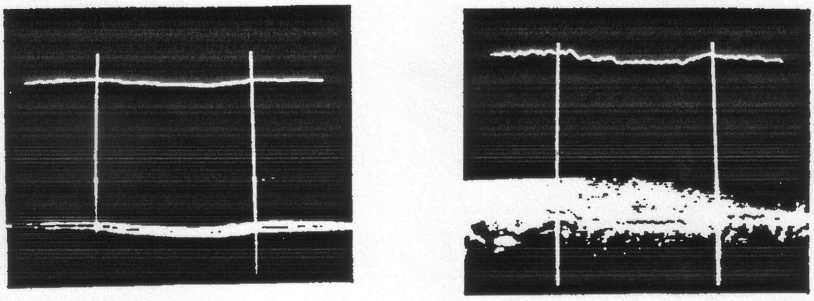

(a) medial axis and feature points

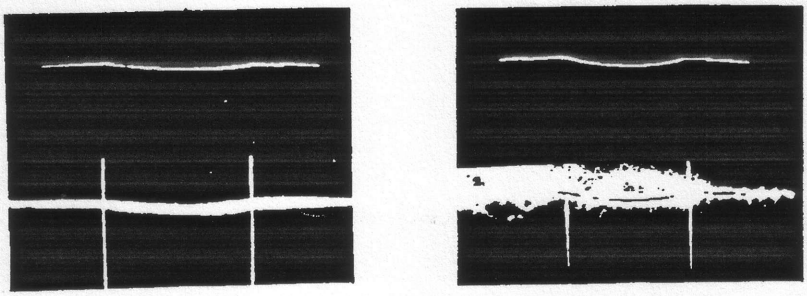

(b) modelled medial axis

Fig.5 Processing of the typical images

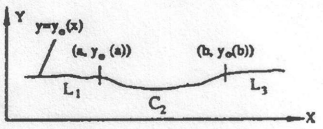

Fig. 6 Medial axis and its feature points

Suppose the equation of the straight line on the left-hand side of a is:

$$y_0=k_0+k_1x+\varepsilon_x, \quad x \le a \tag{1}$$

The curve on the right-hand side of a in a vicinity of a can be approximated by a linear equation:

$$y_0=d_0+d_1 x+\varepsilon_x, \quad x > a \tag{2}$$

where ε_x–$N(0,\sigma^2)$ is the Gaussian white noise representing the error of the medial axis extraction.

Suppose $\hat{a}$ is the horizontal coordinate of a point on the medial axis on the left-hand side of a ($\hat{a} \le a$). We estimate (k_0, k_1) and (d_0, d_1) by the least squares method based on the point set $(\hat{a}-j, y_0(\hat{a}-j))$ $(j=1,2,...,M)$ and $(\hat{a}+j, y_0(\hat{a}+j))$ $(j=1,2,...,M)$, respectively.

According to the maximum principle of the slope difference [15], the following $\hat{a}$ is an unbiased estimate of a:

$$\hat{a}: \max_{\hat{a} \in (a-M, a+M)} (\hat{d}_1(\hat{a})-\hat{k}_1(\hat{a})) \tag{3}$$

Thus, an unbiased recognition algorithm for feature points can be obtained. The resulting algorithm costs about 12 milliseconds. Therefore, our recognition algorithm for the feature points is of real-time as well, for our problem.

The three parts of the medial axis are then fitted to a linear, a quadratic, and a linear model utilizing the least squares method, respectively, progressing from left to right on the image. Suppose the resulting models are $l_1(x)$ $(x \le a)$, $c_2(x, x^2)$ $(a<x<b)$ and $l_3(x)$ $(x \ge b)$, respectively. The point of intersection of l_1 and c_2 is (a^*, y_1^*) ; the point of intersection of c_2 and l_3 is (b^*, y_2^*). Denote the straight line connecting (a^*, y_1^*) and (b^*, y_2^*) as l_2. Then, we can employ the following equations to compute the weld geometric parameters of interest:

Weld width: $$b^*-a^* \tag{4}$$

Average Depression Depth: $$\frac{\int_{a^*}^{b^*} (l_2-c_2)dx}{(b^*-a^*)} \tag{5}$$

Experiments have shown that our real-time processing algorithm developed in this section functions well during actual welding where various noises sometimes are present. Fig.5 illustrates some results of the extracted medial axis, the feature points and the modelled medial axis (l_1, c_2 and l_3). The total time for the image sampling, the image processing and the weld geometric computation is less than 200 milliseconds on our experimental set-up.

Top-side Supervision Parameters

Experiments have been conducted based upon experimental design and based upon emulation of possible variation in welding condition in order to insure the validity of the resulting relationship [16]. Using off-line measurements of top-side parameters with the corresponding back-side weld width, a statistic model:

$$b_b=85.81+4.95h \tag{6}$$

can be obtained by means of the least squares and the F-test (0.05 confidence level), where the variance of the error is $6.23^2 pixel_x^2 (0.31^2\ mm^2)$. The accuracy of this relationship can be shown through comparison between the measured b_b and the model-computed b_b as well (Fig.7). This reveals that b_b can be sufficiently represented by just h. Thus, the top-side average depression depth may be chosen as the top-side supervision parameters of the full penetration state. However, the uniform top-side weld width b should be, in general, obtained during actual welding. Accordingly, both the top-side average depression depth h and the top-side weld width b should be controlled. Therefore, h as well as b are chosen to be the top-side supervision parameters of the full penetration state (the feedback information of the penetration control system) during the actual control.

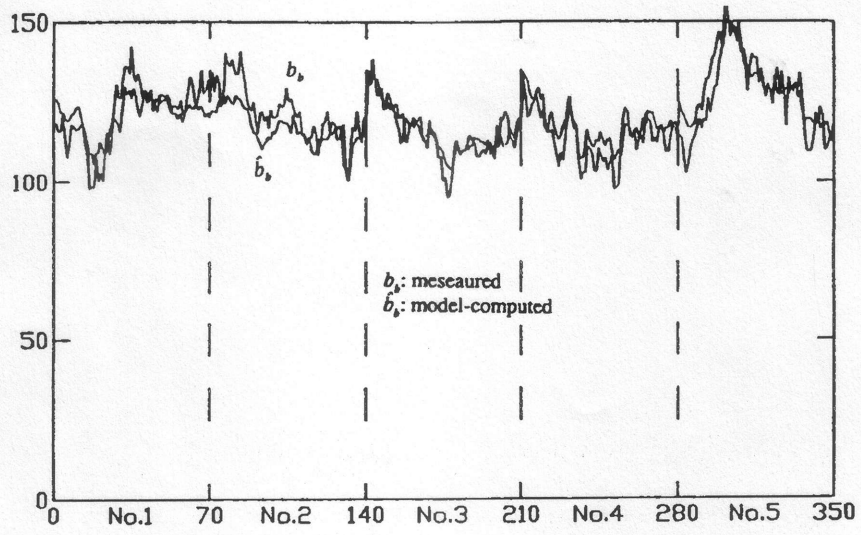

Fig.7 Comparison between the values of measured and model-computed back weld width

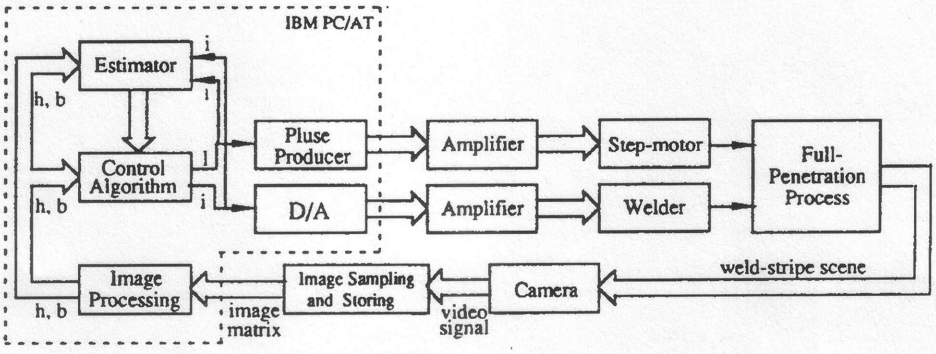

Fig.8 Adaptive control system

Adaptive Predictive Control Principle

The control system is shown in Fig.8. We first model the full penetration process (FPP) which is the controlled process for the control architecture development.

Fig.9 shows a top view of weldpool region at a moment. We have selected the distance from z_3 to z_0 to be 20 millimeters. Also, at z_3, both h and b are extracted by processing the weld image illuminated by the laser stripe. Suppose the view shown in Fig.9 is obtained at the K^{th} sampling instant. At this instant, the laser stripe lies at z_3 (see Fig.9). Let us define: 1) the weld width and the depression at z_3 by $h(k)$ and $b(k)$, respectively; 2) the welding current and arc length at this instant, corresponding to the arc positioned at z_0 (see Fig.9), by $i(k)$ and $l(k)$, respectively. We select MA models as the model structure of the FPP:

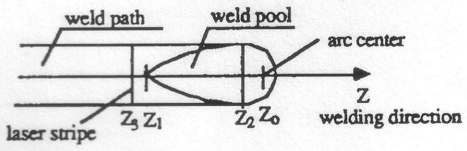

Fig.9 Top-view of the weld pool region

$$\begin{cases} h(k)=b_{10}+\sum_{j=1}^{M_{11}} b_{11}(j)i(k-d_{11}-j)+\sum_{j=1}^{M_{12}} b_{12}(j)l(k-d_{12}-j)+\varepsilon_1(k) \\ b(k)=b_{20}+\sum_{j=1}^{M_{21}} b_{21}(j)i(k-d_{21}-j)+\sum_{j=1}^{M_{22}} b_{22}(j)l(k-d_{22}-j)+\varepsilon_2(k) \end{cases} \quad (7)$$

where z^{-1} is the backshift operator, $\varepsilon_1(k)$ and $\varepsilon_2(k)$ are independent white noise sequences, $M_{ij}(i=1,2,j=1,2)$ are suborders and d_{ij} $(i=1,2, j=1,2)$ are subdelays.

In order to identify model (7), experiments have been conducted under a variety of welding conditions. Using experimental data obtained in a single experiment, an individual model can be obtained. By means of the statistical analysis of all the experimental data, a general model is acquired:

$$\begin{aligned} h'(k)=h(k)-\bar{b}_{10}=&-0.3845\ l(k\text{-}16\text{-}1)+0.0364\ i(k\text{-}9\text{-}1)+\\ &0.0107\ i(k\text{-}9\text{-}2)+0.0214\ i(k\text{-}9\text{-}3)+0.0064\ i(k\text{-}9\text{-}4)+\\ &0.0075\ i(k\text{-}9\text{-}5)+0.0318\ i(k\text{-}9\text{-}6)+0.0240\ i(k\text{-}9\text{-}7)+\\ &0.0406\ i(k\text{-}9\text{-}8)+0.0149\ i(k\text{-}9\text{-}10)+0.0120\ i(k\text{-}9\text{-}11)+\\ &+0.0221\ i(k\text{-}9\text{-}12)+0.0175\ i(k\text{-}9\text{-}12)+\\ &0.0377\ i(k\text{-}9\text{-}13)+\varepsilon_1(k) \end{aligned} \quad (8a)$$

$$\begin{aligned} b'(k)=b(k)-\bar{b}_{20}=&\ 4.17\ l(k\text{-}17)+0.3648\ i(k\text{-}15\text{-}1)+\\ &0.1819\ i(k\text{-}15\text{-}2)+0.1600\ i(k\text{-}15\text{-}3)+\\ &0.1632\ i(k\text{-}15\text{-}4)+0.0564\ i(k\text{-}15\text{-}5)+\\ &0.2155\ i(k\text{-}15\text{-}6)+\varepsilon_2(k) \end{aligned} \quad (8b)$$

where $\bar{b}_{10}$ ($\bar{b}_{20}$) is the mean of b_{10} (b_{20}) in all the individual models, and the variances of ε_1 and ε_2 are 1.200^2 $pixel_y^2$ and 9.193^2 $pixel_x^2$, respectively.

Since practical disturbances of welding conditions are difficult to measure, the best *a priori* description of characteristics of the FPP is given by the general model. As the welding process proceeds the influences of disturbances of welding conditions upon the welding process will become apparent. Although the welding condition can not be measured to decide which typical model should be used, the model can be modified based on the observation of the effect that the welding conditions have upon the process. It is important, therefore, to obtain a better modified model from the initial *a prior* model. However, due to shorter duration of welding, it is difficult to identify all the parameters in (7) on-line. Thus, we present the following model structure (called the real-time model).

$$\begin{cases} h(k)=b_{10}+\lambda_1 h'(k) \\ b(k)=b_{20}+\lambda_2 b'(k) \end{cases} \tag{9}$$

where λ_1 and λ_2 are the so-called gain modification coefficients. During actual welding, λ_j and b_{j0} will be identified on-line. Thus, this real-time model incorporates the general characteristic (described by h' and b') to h, b which are encountered during actual welding.

Based upon the discussion in the last section and some investigation [16], it can be shown that the full penetration process (FPP) is a nonminimum phase plant with high and variable model orders, large and variable delays and variable model parameters. Due to the short welding duration, only few key parameters can be identified on-line instead of all the model parameters, orders and delays. Thus inexact orders and delays will be addressed. Thus, conventional adaptive algorithms such as the generalized minimum variances (GMV) or pole-placement will probably fail if applied to our problem. For example [17], the GMV performs poorly if the plant delay varies, even if it is robust with respect to our assumed model order. Furthermore, other approaches [17] which attempt to estimate the delays using operating data tend to be complex and lack robustness. Moreover, unless special precautions are taken [17], pole-placement and LQG self-tuner are sensitive to the overestimation of the model order due to the pole/zero cancellations in the identified model. However, the generalized predictive control (GPC) presented by Clarke et al. has been shown to be capable of effective control of a plant simultaneously with variable delay, variable order and nonminimum-phase as well as open-loop unstable properties. This algorithm seems to be the most promising for our problem. More information on the GPC can be found in references [17,19].

In our research, an adaptive predictive decoupling control scheme, utilizing GPC as the essential control strategy, is proposed for the FPP (see Fig.10). The control system consists of four essential parts: 1) plant; 2) estimator; 3) predictive control algorithms; 4) decoupling elements. In Fig.10 the plant is the FPP with the welding current and arc length as inputs and the depression and weld width as outputs. The estimator identifies on-line the key parameters in the real time model which include the base values b_{j0} and the gain modification coefficients λ_j (j=1,2), based on the input/output data and feeds the identified results to the predictive control algorithms and the decoupling elements. On basis of the modified model knowledge (i.e. the identified b_{j0} and λ_j) and the set-points of the plant, the predictive control algorithms calculate the generalized welding current $\bar{i}$ and generalized arc length $\bar{l}$, which are inputs of the decoupling elements. Finally, in Fig.10, the decoupling elements compute the welding current i and arc length l, which are actual inputs of the plant, based on the modified model knowledge and both the generalized welding current $\bar{i}$ and the generalized arc length $\bar{l}$.

In order to determine the controller's parameters, simulations under a variety of welding conditions (which are emulated by a variety of individual mathematical models) have been conducted.

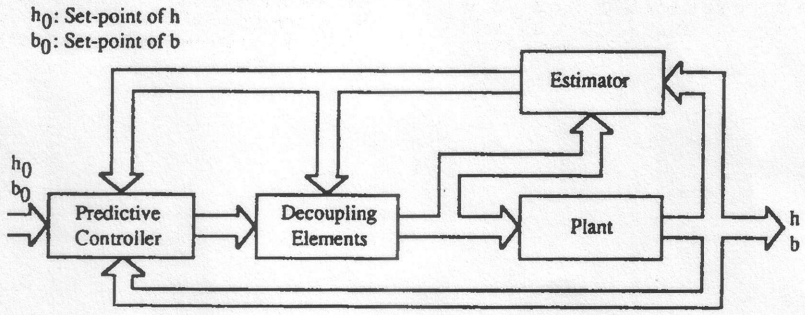

Fig.10 Predictive decoupling control principle

Experiments

As mentioned previously, our research addresses the presentation and realization of a novel top-side control strategy for the full penetration state in full penetration gas tungsten arc welding. As the last stage of the whole research work, the experiments are actually a general examination of 1) the relationship between the top-side and back-side weld geometric parameters based on which h and b are selected as the top-side supervision parameters of the full penetration state; 2) the developed three dimensional vision sensor (hardware and algorithm) by which the weld image with laser stripe is acquired and processed to calculate h and b ; 3) the developed control equipment; 4) the modelling of the FPP, and 5) the developed control scheme.

Experiments under a variety of variable welding conditions have been performed [16]. These experiments have demonstrated the excellent performance of the developed control scheme. Fig.11 and 12 show the compared experiments under variable heat transfer circumstance between an open-loop control strategy and the adaptive predictive control strategy. It can be seen that in Fig.11, h and b_s are influenced by the heat transfer circumstance. However, in Fig.12, this influence is overcome by the correspondingly changed i and l.

Conclusions

The average depression depth is proposed to be a geometric parameter of the cross section of full penetration welds. A linear relationship exists between the full penetration state (the back-side weld width) and the top-side average depression depth. However, in order to obtain an uniform weld, both the top-side average depression depth and the top-side weld width are taken as the top-side supervision parameters (outputs) of our full penetration control system.

A structured-light 3D vision sensing system has been developed to measure the top-side weld geometric parameters in GTA welding. A real-time image processing technique has been presented to acquire accurate weld geometric parameters during actual welding. This technique depends on two novel image processing algorithms: an adaptive dynamic algorithm which extracts the medial axis of the laser stripe, and an unbiased algorithm which recognizes the feature points of the medial axis.

Based upon the input-output data pair of dynamic experiments, both individual models and the general model are built. A real-time control model with fewer key parameters to be identified on-line is presented for the implementation of adaptive control.

In the adaptive control of the FPP (which is with simultaneous larger and variable orders, larger and variable delays,

nonminimum-phased property and shorter duration of process), the real time model, the GPC, and the predictive decoupling algorithm have played key roles. The excellent performance of the developed control scheme have been demonstrated by simulation and experiment, both of which are were performed under various possible disturbances in our studies.

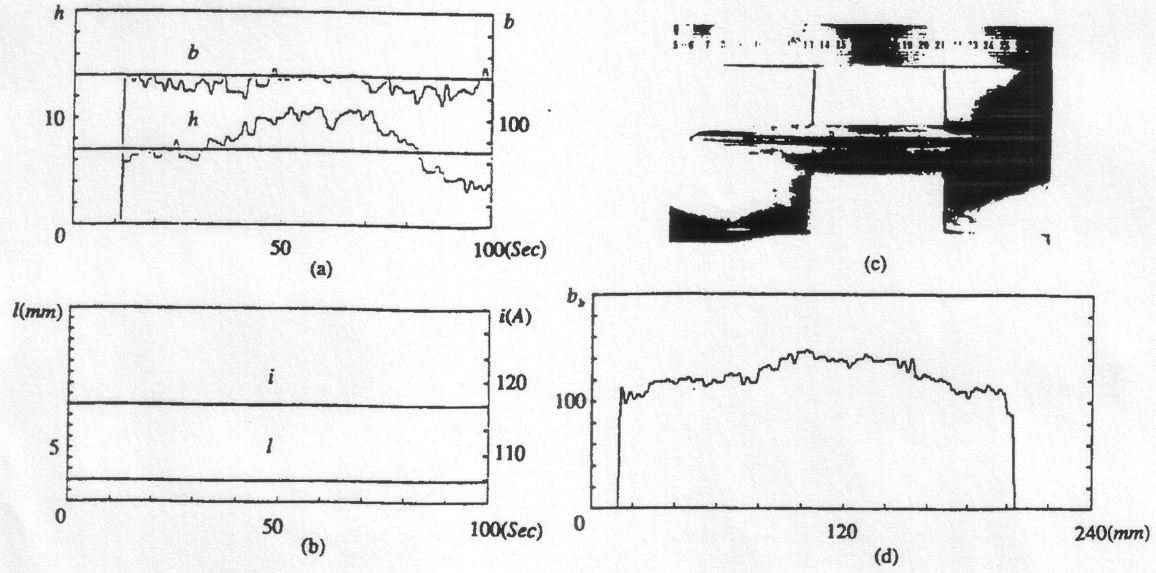

Fig.11 Bead-on-plate experiment under varying heat transfercircumstance: $\theta = 60^0$(open loop)
(a) on-line top-side measurements (b) control signals
(c) back-side photograph (d) off-line back-side measurements

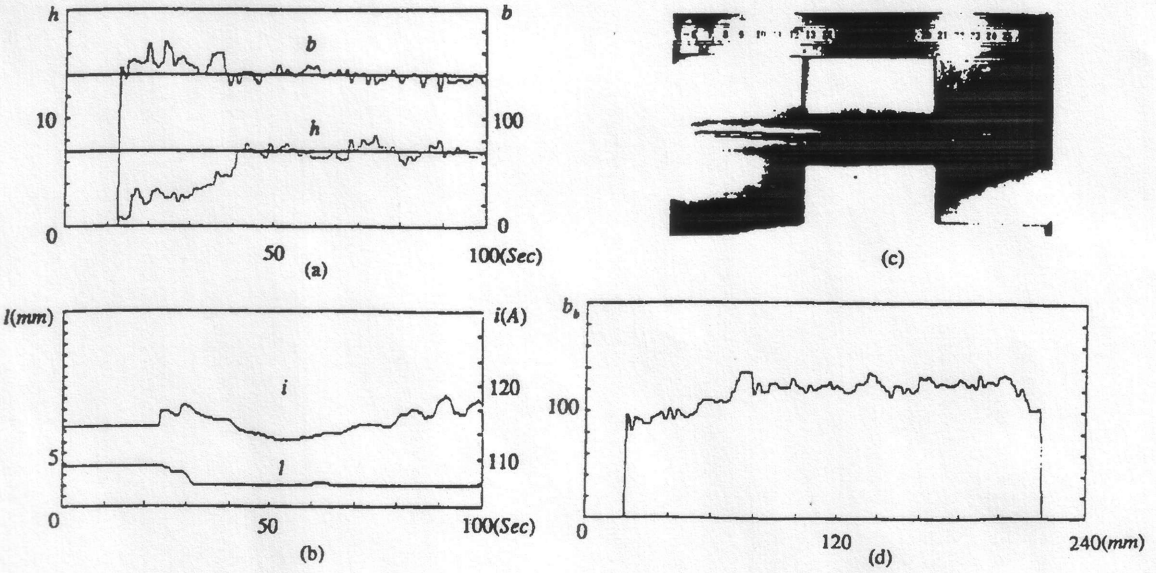

Fig.12 Bead-on-plate experiment under varying heat transfercircumstance $\theta = 60^0$(closed-loop)
(a) on-line top-side measurements (b) control signals
(c) back-side photograph (d) off-line back-side measurements

References

[1] Hardt, D. E. et al. 1982. Improvement of Fusion Welding Through Modelling, Measurement, and Real-Time Control. International Conference on **Welding Technology for Energy Applications**, Gatlinburg, TN, May 1982

[2] Renwick, R. J. and Richardson, R. W. 1983. Experimental Investigation of GTA Weld Pool Oscillations. **Welding Journal**, Vol.62, No.2

[3] Zacksenhouse, M. and Hardt, D. E. 1984. Weld pool Impedance Identification for Size Measurement and Control. **Journal of Dynamic Systems, Measurement and Control**, Vol.105, No.3, Sept.

[4] Sorensen, C. D. 1985. Digital Signal Processing as a Diagnostic Tool for Gas Tungsten Arc Welding. Ph.D. Thesis, MIT Department of Material Science, May

[5] Hardt. D. E. 1986. Measuring Weld pool Geometry from Pool Dynamics. Modeling and Control of Casting and Welding, ASM, Jan. 1986

[6] Tam, A. S. and Hardt D. E. 1989. Weld Pool Impedance for Pool Geometry Measurement: Stationary and Nonstationary Pools. **Journal of Dynamic Systems, Measurement and Control**, Vol.111, No.4, pp.545-553, Dec.

[7] Xiao, Y. H. and Ouden G.den 1990. A Study of GTA Weld Pool Oscillation. **Welding Journal**, Vol.69, No.8, pp298s-293s

[8] Hardt, D.E. and Katz, J.M. 1984. Ultrasonic Measurement of Weld Penetration. **Welding Journal**, Vol.63, No.9, pp.273s-281s

[9] Lott, L. A. 1983. Ultrasonic Detection of Molten/Solid Interfaces in Weld Pools. **Material Evaluation**, Vol.42:337-341

[10] Lott, L. A., Johnson, J. A., and Smartt, H. B. 1984. Real-Time Ultrasonic Sensing of Arc Welding Process. Proceedings, 1983 Symposium on nondestructive Evaluation Applications and Materials Processing, pp. 13-22, Metals Park, Ohio, ASM International

[11] Johnson, J. A., Carlson, N. M., and Lott. L. A. 1988. Ultrasonic Wave Propagation in Temperature Gradients. **Journal of Nondestructive Evaluation**, Vol.6, No.3, pp147-157

[12] Carlson, N. M. and Johnson, J. A. 1988. Ultrasonic Sensing of Weld Pool Penetration. **Welding Journal** Vol.67, No.11, pp239s-246s

[13] Nagarajan, S., Chen, W.H. and Chin, B.A. 1989. Infrared Sensing for Adaptive Arc Control. **Welding Journal**, Vol.68, No.11, pp.462s-466s

[14] Chen, W. and Chin, B.A. 1990. Monitoring Joint Penetration Using Infrared Sensing Techniques. **Welding Journal**, Vol.69, No.4, pp181s-185s

[15] Schalkoff, R. J. 1989. Digital Image Processing and Computer Vision, Johnwiley & Sons, Inc. (p22)

[16] Zhang, Y.M. 1990. Adaptive Top-Vision Full Penetration Control in TIG Welding, Ph.D. Dissertation, Harbin Institute of Technology, China

[17] Clarke, D.W., Mohtadi, C., and Tuffs, P.S. 1987. Generalized Predictive Control – Part 1. The Basic Algorithm, **Automatica**, vol.23,no.2,pp.137-148

[18] Kurz, H. and Goedecke 1981. Digital Parameter-adaptive Control of Process with Unknown Dead Time, **Automatica**, Vol.17, pp.245-252

[19] Clarke, D. W. and Mohtadi, C. 1989. Properties of Generalized Predictive Control, **Automatica**, Vol.25, No.6